Vibronic Thulium Laser at 2131 nm Q-switched by Single-Walled Carbon Nanotubes

P. Loiko,[1,2] X. Mateos,[1,3,*] S. Y. Choi,[4] F. Rotermund,[4] J. M. Serres,[1] M. Aguiló,[1] F. Díaz,[1] K. Yumashev,[2] U. Griebner,[3] and V. Petrov[3]

[1]*Física i Cristal·lografia de Materials i Nanomaterials (FiCMA-FiCNA), Universitat Rovira i Virgili (URV), Campus Sescelades, c/ Marcel·lí Domingo, s/n., E-43007 Tarragona, Spain*
[2]*Center for Optical Materials and Technologies, Belarusian National Technical University, 65/17 Nezavisimosti Ave., 220013 Minsk, Belarus*
[3]*Max Born Institute for Nonlinear Optics and Short Pulse Spectroscopy, Max-Born-Str. 2a, D-12489 Berlin, Germany*
[4]*Department of Physics & Department of Energy Systems Research, Ajou University, San 5 Wonchun-dong, 443-749 Suwon, Republic of Korea*
**Corresponding author: xavier.mateos@urv.cat, mateos@mbi-berlin.de*

Received XX Month XXXX; revised XX Month, XXXX; accepted XX Month XXXX; posted XX Month XXXX (Doc. ID XXXXX); published XX Month XXXX

Efficient and power-scalable laser operation of a vibronic Tm^{3+}:$KLu(WO_4)_2$ microchip laser at ~2.13 μm is demonstrated. In the continuous-wave mode under diode pumping at ~805 nm, this laser generated 1.17 W at 2109–2133 nm with a slope efficiency of 39%. This emission is related to the coupling of the electronic transitions of Tm^{3+} ions with the stretching vibrations of the WOW oxygen bonds in the monoclinic $KLu(WO_4)_2$ crystal host appearing at ~379, 406 and 450 cm^{-1}. The achieved emission wavelength is longer than any previously reported laser based both on Tm^{3+} or Ho^{3+} doped double tungstate crystals. Passive Q-switching of the vibronic Tm^{3+}:$KLu(WO_4)_2$ laser is realized with a single-walled carbon nanotubes (SWCNT) based saturable absorber (SA) representing the longest wavelength in this mode of operation. In this regime, the maximum output power reached 0.70 W at 2131 nm corresponding to a slope efficiency of 29%. The pulse characteristics were 25 ns / 1.1 μJ at the pulse repetition frequency of 0.62 MHz. These are the shortest pulses ever achieved in any lanthanide based laser passively Q-switched by carbon nanostructures. A conventional (purely electronic transition) Tm^{3+}:$KLu(WO_4)_2$ microchip laser at 1.92 μm Q-switched by the same SWCNTs generated 40 ns / 4.0 μJ pulses corresponding to a peak power of 0.1 kW which is a record value for this type of laser oscillators. © 2016 Optical Society of America

OCIS codes: *(140.3070) Infrared and far-infrared lasers; (140.3540) Lasers, Q-switched; (140.3380) Laser materials.*

http://dx.doi.org/10.1364/AO.99.099999

1. INTRODUCTION

Eye-safe lasers emitting at around 2 μm are of practical importance for remote sensing of CO_2 and H_2O vapor in the atmosphere (LIDAR technology), metrology and laser surgery [1]. Such lasers are also used for pumping of mid-IR optical parametric oscillators (OPOs) [2]. The 2 μm laser emission is usually achieved from thulium (Tm^{3+}) or holmium (Ho^{3+}) ions and assigned to the $^3F_4 \rightarrow {}^3H_6$ and $^5I_7 \rightarrow {}^5I_8$ electronic transitions within the $4f^n$ shell, respectively [3,4]. Tm lasers normally emit at wavelengths slightly below 2 μm while the Ho ones can operate above 2 μm. Both types of lasers exhibit wide tunability range of their emission (~200 nm at zero-level) [3]. Laser emission above 2 μm has some advantages: it better matches the water absorption which is relevant for reducing the penetration depth into bio-tissues, and it corresponds to weaker residual absorption in the non-oxide nonlinear crystals used in OPOs [2].

Although Ho lasers can provide the desired emission beyond 2 μm, their design (and, in particular, pumping) is more complicated as compared with their Tm counterparts. Tm^{3+} ions have a strong absorption band at ~0.8 μm ($^3H_6 \rightarrow {}^3H_4$ transition) which matches the emission of commercial high-power AlGaAs laser diodes [5]. In addition, an efficient cross-relaxation (CR) mechanism between adjacent Tm^{3+} ions, $^3H_4 + {}^3H_6 \rightarrow {}^3F_4 + {}^3F_4$, increases the quantum efficiency of the excitation up to ~2 (i.e., one can potentially achieve two ~2 μm laser photons from one pump photon) [6], and consequently reduces strongly the heat loading in the crystal. The Ho^{3+} ions show relatively small absorption oscillator strengths [7]. They can be excited via the Tm → Ho energy-transfer (ET) in the (Tm^{3+}, Ho^{3+}) couple [4,8]. However, strong upconversion is observed in codoped materials that leads to a reduction of the laser efficiency [9]. Resonant (in-band) excitation of the Ho^{3+} ions to the $^5I_7$ upper laser level by Tm fiber or bulk lasers is also possible [10,11] eliminating the drawback of upconversion but still suffering from poor pump efficiency due to the low Ho absorption. Thus,

the design of Tm lasers which can operate at wavelengths beyond 2 μm is of high importance.

To a certain extent, the emission range of Tm lasers can be managed by an appropriate host which can result in various Stark splitting of the ground- and excited-state multiplets. In particular, Tm-doped BaY_2F_8 [12], $LiLuF_4$ [13], $LiGdF_4$ [14] and $YAlO_3$ [15] crystals provide emission up to ~2.03 μm, while Tm:Lu_2O_3, Tm:Sc_2O_3 [16,17] and Tm: $Y_3Sc_2Ga_3O_{12}$ [3] operate even at >2.1 μm. Laser oscillation at such long wavelengths originates partially from the coupling of the electrons that participate in the $^3F_4 \rightarrow {}^3H_6$ electronic transition with the active phonons (vibrations) of the host [12,18]. A vibronic laser emission relies on the electron-phonon coupling. This effect is particularly strong for ions located in the beginning (Pr^{3+}) and in the end (Yb^{3+},Tm^{3+}) of the lanthanide series [19,20]. Long-wavelength vibronic laser operation is achieved normally by the insertion of a wavelength-selective optical element (e.g., a birefringent filter) into the laser cavity or using cavity mirrors with selective coating.

Recently, vibronic operation at >2 μm without intracavity elements was observed in a highly-doped Yb,Tm:$KLu(WO_4)_2$ laser [18,21]. This crystal belongs to the family of monoclinic double tungstates (DTs) with the chemical formula $KRE(WO_4)_2$ or shortly KREW where RE = Gd, Y or Lu [22]. DTs are very suitable for Tm doping [23,24]. Among them, particularly KLuW is the most attractive host due to the closeness of the ionic radii of the VIII-fold oxygen-coordinated Lu^{3+} (0.977 Å) and Tm^{3+} (0.994 Å) ions. Tm:KLuW crystals show high transition cross-sections with polarized light, as well as relatively broad absorption bands [23]. An efficient CR in Tm:KLuW crystals is observed even at low doping levels (3 at.%) [6], which results in low heat loading [25]. In addition, high doping in the isostructural series $KTm_xLu_{1-x}W$ is possible accomplished by weak luminescence quenching and excellent optical quality of the crystals [26]. As a result, efficient continuous-wave (CW) [26-28], passively Q-switched (PQS) [29,30] and mode-locked [31] Tm:KLuW lasers have already been demonstrated.

An important advantage of KLuW as a host crystal is that it provides attractive thermo-mechanical properties: higher thermal conductivity (~3 W/mK) [32] and lower anisotropy of the thermal expansion coefficient [33], as compared with its KGdW and KYW counterparts. Although KLuW possesses negative dn/dT coefficients [34], athermal crystal cuts resulting in positive thermal lens exist for this crystal [33]. The latter is crucial for the design of Tm microchip lasers with the gain material and (optionally) saturable absorber (SA) both placed in a compact plano-plano cavity [35]. CW or PQS microchip lasers are beneficial due to the compact and robust design, low intracavity losses and the possibility to generate short laser pulses via the reduction of the cavity roundtrip time [36,37]. Power scaling of CW Tm:KLuW microchip lasers has been reported [35,38], and the generation of short pulses in PQS Tm:KLuW microchip lasers when using bulk (Cr^{2+}:ZnS) [30] and nanostructured (graphene) [39] SAs demonstrated as well.

Low losses in the microchip laser are beneficial for the observation of efficient vibronic coupling [21]. In the present work, we report on CW and PQS Tm:KLuW vibronic microchip lasers operating at ~2.13 μm. This laser wavelength is much longer than the typical emission wavelength of Tm^{3+} (~1.95 μm) and even Ho^{3+} (~2.06–2.08 μm) ions in KLuW. As a SA, we applied single-walled carbon nanotubes (SWCNTs), for the first time at such long wavelengths. The SWCNTs emerge as broadband SAs for near-IR lasers [40,41] as they show low saturation fluence, low non-saturable losses, ultrafast recovery time and relatively high laser damage threshold. The results achieved in the present work with the vibronic PQS Tm:KLuW/SWCNT laser represent the shortest pulses ever achieved with near-IR lasers PQS by carbon nanostructures.

2. EXPERIMENTAL

A. Laser set-up

Tm:KLuW is a monoclinic crystal (space group $C2/c \equiv C^6_{2h}$, point group $2/m$). It was grown by the Top-Seeded Solution Growth (TSSG) Slow-Cooling method using potassium ditungstate, $K_2W_2O_7$, as a solvent, and a [010]-oriented seed [22]. The Tm content in the solution was 3 at.% and the actual Tm concentration measured by Electron Probe Micro Analysis (EPMA) was $N_{Tm} = 2.15\times10^{20}$ cm^{-3}.

Tm:KLuW is optically biaxial. Its optical properties are described in the frame of the optical indicatrix with the principal axes, N_p, N_m and N_g (for which the corresponding refractive indices are $n_p < n_m < n_g$). For microchip operation, only the crystal cut along the N_g-axis can be used. It corresponds to a positive thermal lens, which is required for the laser mode stabilization in the plano-plano cavity [42]. The N_g-cut Tm:KLuW crystal was 3.0-mm-thick. Both $m\times p$ crystal faces with dimensions 3.0×3.0 mm^2 were polished to laser quality and remained uncoated. The laser crystal was mounted in a Cu-holder using Indium foil to provide good thermal contact from all 4 lateral sides. The holder was water-cooled at 12°C.

The laser cavity was composed of a flat pump mirror (PM) that was antireflection (AR) coated for 0.8–1.0 μm and high-reflection (HR) coated for 1.8–2.15 μm and a flat output coupler (OC), Fig. 1(a). We used two OCs: a "standard" one which provided a transmission of T_{OC} = 10% at 1.8–2.1 μm and a special "bandpass" OC with high transmission (T > 80%) at 1.9–1.97 μm and T_{OC} =1.6% at 2.05–2.20 μm. The transmission-type SA was inserted into the cavity between the crystal and the OC. The cavity contained no air gaps and thus its total geometrical length was ~4 mm. The cavity length was minimized in order to reduce the cavity roundtrip time.

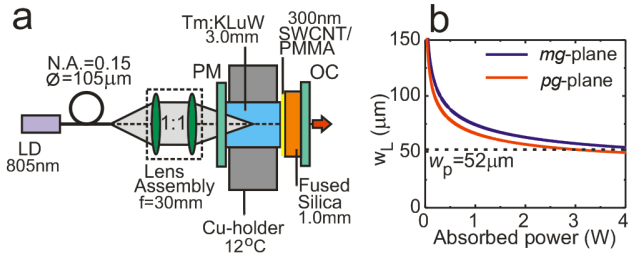

Fig. 1. (a) Scheme of the PQS Tm:KLuW vibronic microchip laser: LD - laser diode, PM - pump mirror, OC - output coupler; (b) calculated radii of the laser mode w_L in the crystal versus the absorbed pump power, w_p is the mean radius of the pump beam.

The crystal was pumped in a single pass by an AlGaAs fiber-coupled laser diode (Intense Ltd, fiber core diameter: 105 μm, N.A. = 0.15) emitting at λ_p = 805 nm ($^3H_6 \rightarrow {}^3F_4$ transition of Tm^{3+}). The unpolarized pump radiation was reimaged into the crystal with a lens assembly (1:1 ratio, 30 mm focal length). The pump spot size in the crystal was w_p = 52±5 μm. The M^2 parameter for the pump beam was estimated as $M^2 = \pi w_p \times N.A./\lambda_p \sim 31$. The confocal parameter for the pump beam was then $2z_R = 2\pi w_p^2 n/(\lambda_p M^2)$= 1.3 mm. The absorption of the pump radiation in the crystal under lasing conditions was ~32%.

The radius of the laser mode in the crystal w_L was calculated with the ABCD-method, Fig. 1(b). Previously reported thermo-optic parameters of Tm:KLuW were used for the simulation: M = 12.9 m^{-1}/W and 8.1 m^{-1}/W for the *pg* and *mg* principal meridional planes, respectively (for w_p = 100 μm and $E \,||\, N_m$) [42]. Here, $M = dD/dP_{abs}$ are the sensitivity factors of the thermal lens, P_{abs} is the absorbed pump power, $D = 1/f$ is the optical (refractive) power of the lens and f is its

focal length. The *M*-factor is inversely proportional to the transverse area of the pump beam ($M \sim 1/w_p^2$). Taking this into account, we calculated focal lengths of the lens at the maximum applied P_{abs} of ~4 W, f = 5 and 8 mm for the *mg*- and *pg*-planes, respectively.

A fast InGaAs PIN photodetector (EPS Inc., model ET-5000, response time: ~30 ps) and 1 GHz digital oscilloscope (LeCroy, model Wave Surfer 104Xs-A) were used for detection of the Q-switched pulses.

B. Saturable absorber

Purified SWCNTs synthesized by the arc-discharge method were used in our studies. The scanning electron microscope (SEM) image of the SWCNTs spray-coated onto a Si wafer is shown in Fig. 2(a). To fabricate the SA, the SWCNT/PMMA film was spin-coated onto an uncoated ~1-mm-thick quartz substrate (film thickness: ~300 nm), see details in [41]. The individual SWCNTs are well distributed in the film and randomly oriented (spaghetti-like).

The transmission spectrum of the SWCNT SA is shown in Fig. 2(b). In the spectrum, two broad bands spanning from ~0.8 to 1.2 μm and from ~1.6 to 2.3 μm are observed. The second band is related to the first fundamental transition of semiconducting carbon nanotubes (denoted as E_{11}). It is used for the PQS of the Tm:KLuW laser. The first band is related to the second van Hove optical transition (E_{22}) of semiconducting carbon nanotubes. The weakly pronounced structure and width of both absorption bands are attributed to the absorption of nanotubes with slightly different diameters spanning from 1.5 up to 2.2 nm.

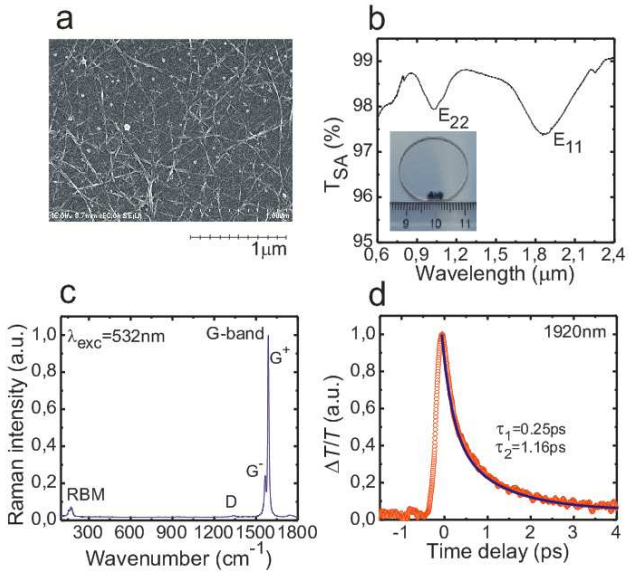

Fig. 2. SWCNT SA: (a) SEM image of the arc-discharge SWCNTs spray-coated onto a Si wafer; (b) transmission spectrum of the SA, Fresnel losses are subtracted (*inset* - image of the SA); (c) Raman spectrum of the SA, excitation wavelength is 532 nm; (d) recovery of the initial absorption for the SA measured by the pump-probe technique at 1920 nm, τ_1 and τ_2 are the characteristic times of the bi-exponential fit (blue curve).

The Raman spectrum of the SA is shown in Fig. 2(c). The spectrum contains the characteristic bands of SWCNTs [43]. The structured band composed of several peaks at 157, 171, 176 and 186 cm^{-1} is the radial breathing mode (RBM) attributed to nanotubes of different diameter. A very intense G-band is the optical phonon mode of graphite materials including graphene and carbon nanotubes. For SWCNTs, it is composed of several peaks due to the phonon vibration along the circumferential or nanotube axis direction. The split G-band is also a distinctive feature of cylindrically rolled graphene – SWCNTs, where G^+ is the higher frequency component which corresponds to the carbon atom vibration along the nanotube axis, and G^- is the lower frequency one which arises from the vibration along the circumferential direction [43].

The small-signal absorption of a SWCNT SA is $\alpha'_{SA} = 1 - T_{SA}$ where T_{SA} is its intrinsic small signal transmission, i.e. obtained by subtracting the Fresnel losses. The SWCNTs show absorption saturation under short-pulse excitation [40]:

$$\alpha'_{SA}(I_L) = \alpha'_{NS} + \frac{\alpha'_S}{1+(I_L/I_{sat})}, \quad (1)$$

where α'_{NS} and α'_S are the non-saturable and saturable parts, respectively, I_L is the laser intensity on the SA and I_{sat} is the saturation intensity. In our case, I_L means the peak on-axis intracavity laser intensity. In the assumption of TEM_{00} laser mode and nearly Gaussian temporal profile of single pulses, $I_L = X[2E_{out}/\pi w_L^2 \tau^*]$, where $X = (1+R_{OC})/(1-R_{OC})$ and R_{OC} is the reflectivity of the OC, E_{out} is the output pulse energy, the term "2" indicates a Gaussian spatial profile and $\tau^* \approx 1.06\tau$ (τ: FWHM intensity) is the effective pulse duration.

Recently, we have estimated I_{sat} for the SWCNT-SA of 7±1 MW/cm^2 at ~2.1 μm (E_{11} transition) for the ns-long laser pulses [44]. Relatively low saturation intensity of the SWCNT-SA at ~2 μm is beneficial for its deep saturation when employed in the Tm:KLuW laser. The fraction of saturable losses, α'_S/α'_{SA}, was estimated at ~2.1 μm as ~0.21 [44]. For the considered SA, the small signal absorption α'_{SA} amounts to 2.5% and 1.5% at ~1.92 and 2.13 μm, respectively. Thus, the maximum modulation depth of the SWCNT-SA at these two wavelengths is 0.52% and 0.32%, respectively. The ultrafast recovery of the initial absorption of the SWCNT-SA, Fig. 2(d), was studied by the pump-probe technique at ~1.9 μm [45], yielding two recovery times τ_{rec}, "fast" with τ_1 = 0.25 ps and "slow" with τ_2 = 1.16 ps.

3. RESULTS AND DUSCUSSION

At first, we studied the CW operation of the Tm:KLuW laser without the SA in the cavity, Fig. 3(a). The absorbed pump power was limited to P_{abs} <4 W in order to avoid thermal fracture of the crystal. With the 10% OC, the maximum output power reached 2.11 W at ~1921 nm corresponding to a slope efficiency η = 63% (with respect to the absorbed power). The laser threshold was at P_{abs} = 0.48 W and the optical-to-optical efficiency amounted to η_{opt} = 55%. The laser output was linearly polarized along the N_m-axis, and the polarization was naturally-selected by the anisotropy of the gain [23].

With the "bandpass" OC, laser oscillation occurred at 2109-2133 nm (multi-peak spectrum). The maximum output power reached 1.17 W corresponding to a lower slope efficiency η = 39% (η_{opt} = 31%) and an increased laser threshold, P_{abs} = 0.82 W. The laser output was only partially polarized (with the predominant direction of polarization along the N_m-axis) which is a clear indication of vibronic nature of laser transition [12]. For both OCs, the output dependences were clearly linear showing no detrimental influence of the thermal effects.

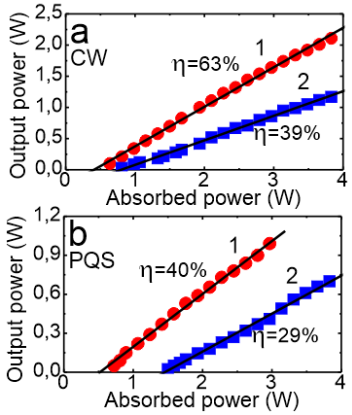

Fig. 3. Input-output dependences for the CW (a) and PQS (b) Tm:KLuW laser at 1.92μm (10% OC) (1) and 2.13 μm (1.6% bandpass OC) (2), η – slope efficiency.

Excellent stability in PQS operation was achieved with both OCs. The corresponding output dependences are shown in Fig. 3(b). For the 10% OC, the laser generated 0.99 W at ~1919 nm with η = 40%. Due to the insertion loss of the SA, the laser threshold increased to ~0.66 W. The conversion efficiency with respect to the CW operation mode was η_{conv} = 60%. With the "bandpass" OC, the laser operated at 2131 nm with maximum output power of 0.70 W and η = 29%. In this case, the laser threshold increased to ~1.5 W and the Q-switching conversion efficiency was nearly the same as for 10% OC, η_{conv} ~60%. For both OCs, the polarization behavior of the laser was as in the CW mode.

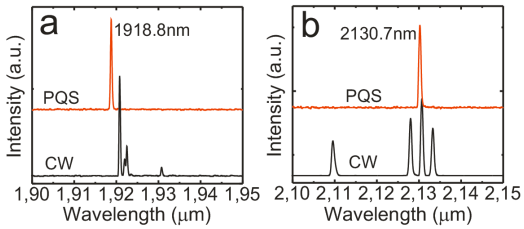

Fig. 4. Typical laser emission spectra for CW and PQS operation of the Tm:KLuW laser with 10% OC (a) and 1.6% bandpass OC (b), P_{abs} = 2.9 W.

The laser emission spectra of the Tm:KLuW laser in CW and PQS operation modes are shown in Fig. 4. In order to interpret them, we plotted the absorption σ_{abs} and stimulated-emission (SE) σ_{SE} cross-section spectra of Tm:KLuW for light polarization $E \parallel N_m$ corresponding to the $^3H_6 \leftrightarrow {}^3F_4$ transition, see Fig. 5(a). Here, the spectral dependence of σ_{SE} is derived with the reciprocity method based on the experimental absorption spectrum and the Stark splitting of the involved multiplets. It indicates that the electron-phonon coupling is responsible, in particular, for the long-wavelength tail of the SE cross-section spectrum [7]. From Fig. 5(a), the gain cross-sections, $\sigma_g = \beta\sigma_{SE} - (1-\beta)\sigma_{abs}$ was derived, where β is the inversion ratio (N_2/N_{Tm}, N_2 is the population density of the emitting state, $^3F_4$), as shown in Fig. 5(b). At very low β < 0.05, the gain cross-section spectrum is flat and broad (1970–2050 nm). With the increase of the inversion ratio, two local peaks are formed in the spectrum, centered at ~1945 nm and 1918 nm. Laser oscillation around the second peak is expected for β > 0.3 (in other words, relatively large cavity losses either due to output coupling or to intracavity elements). Thus, the spectra in Fig. 4(a) for CW and PQS operation with the 10% OC correlate well with the gain spectra, Fig. 5(b).

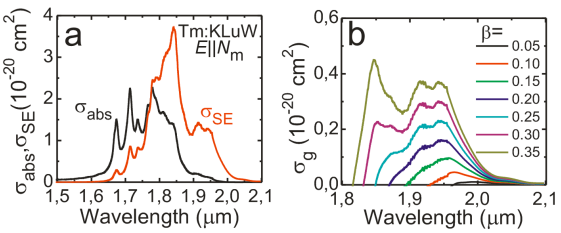

Fig. 5. (a) Absorption, σ_{abs}, and stimulated-emission, σ_{SE}, cross-sections and (b) gain cross-sections, $\sigma_g = \beta\sigma_{SE} - (1-\beta)\sigma_{abs}$, for Tm^{3+} ions in KLuW for light polarization $E \parallel N_m$, β is the inversion ratio.

From the gain cross-sections spectra, Fig. 5(a), the longest laser wavelength expected from Tm:KLuW is 2.05 μm, in contrast to the observed emission when using the "bandpass" OC, Fig. 4(b). As mentioned above, the long-wavelength emission in Fig. 4(b) is mainly due to the electron-phonon coupling which is typical for Tm^{3+} lasers. Indeed, according to the Stark splitting of the $^3H_6$ and $^3F_4$ multiplets of Tm^{3+} ions in KLuW [23], shown in Fig. 6(b), the longest wavelength of a purely electronic $^3F_4 \rightarrow {}^3H_6$ transition is 1948 nm. It corresponds to the transition from the lowest Stark level of the $^3F_4$ multiplet (5663 cm^{-1}) to the highest Stark level of the $^3H_6$ one (530 cm^{-1}). However, using a long pass filter such as the "bandpass" OC, emission at even longer wavelengths is observed. This is attributed to a coupling of the electrons that participate in the electronic transition $^3H_6 \rightarrow {}^3F_4$, with various phonons of the host, i.e. vibronic coupling. The relaxation of a Tm^{3+} ion excited to the $^3F_4$ level may lead to the excitation of a phonon of the crystalline host and the emission of one photon with lower energy (longer wavelength) than the one expected from a purely electronic transition. This effect can be described also in terms of virtual energy levels obtained by adding the phonon energies to the Stark sub-levels of the $^3H_6$ ground-state of Tm^{3+} ion [18], Fig. 6(c). Thus, the emission from the vibronic laser can be considered as transitions from the upper laser level ($^3F_4$) to one such virtual energy state (lower laser level). To date, vibronic laser emission has been detected in free-running mode from several Tm^{3+}-doped fluoride crystals, e.g. BaY_2F_8, $LuLiF_4$ and $GdLiF_4$ [12-14], under diode-pumping, as well as when using birefringent filter for tuning of the laser emission with Tm^{3+}-doped oxides such as $Y_3Sc_2Ga_3O_{12}$, $GdVO_4$, Lu_2O_3 or $YAlO_3$ [3,15,16].

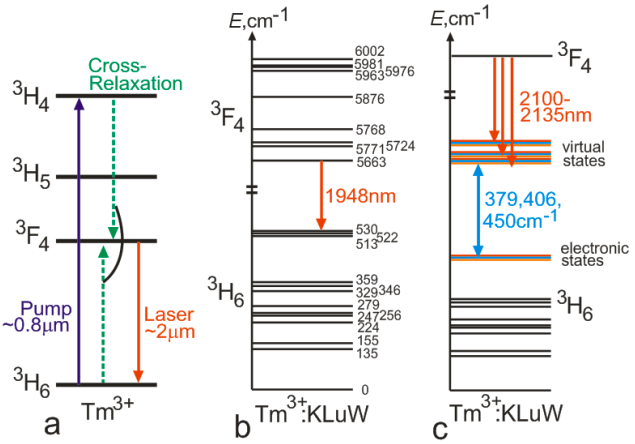

Fig. 6. Energy levels of the Tm^{3+} ion: (a) simplified scheme; (b) Stark splitting of the $^3F_4$ and $^3H_6$ multiplets in KLuW [23], *arrow* denotes the

longest-wavelength purely electronic transition; (c) scheme illustrating the position of virtual states for the Tm^{3+} ion due to coupling with vibrations of the KLuW host (in color) participating in the laser emission at ~2.1 μm.

In order to explain the emission at 2109-2133 nm from the Tm:KLuW laser, we refer to the Raman spectra of KLuW. The polarized Raman spectra of the N_g-cut Tm:KLuW crystal are shown in Fig. 7 for the $g(xy)g$ geometries (where x and $y = m$ or p). Here, we use the standard notations for Raman spectroscopy: first and last indices indicate the propagation direction of the excitation and scattered light, and the indices in brackets stand for the corresponding polarizations. The phonons below 240 cm^{-1} are assigned to external lattice modes associated with translational motion of the cations T'(K^+, Lu^{3+} and W^{6+}) and rotational motion of the WO_6 groups; the bending modes δ are observed in the 290–350 cm^{-1} range, and the stretching modes ν in the 380–910 cm^{-1} range [46], see Table 1 for details. In previous work, the emission slightly above ~2 μm of vibronic Tm:KLuW lasers was attributed to the low-energy vibrations at 147, 176, 218 and 236 cm^{-1} [18,21]. For the present laser, the involved vibrations are those at ~379, 406 and 450 cm^{-1}. If coupled to the higher-lying Stark sub-levels of the $^3H_6$ state (~513, 522 and 530 cm^{-1}), these modes may generate virtual states resulting in stimulated emission with wavelengths as long as 2.10-2.13 μm, as illustrated in Fig. 6(c).

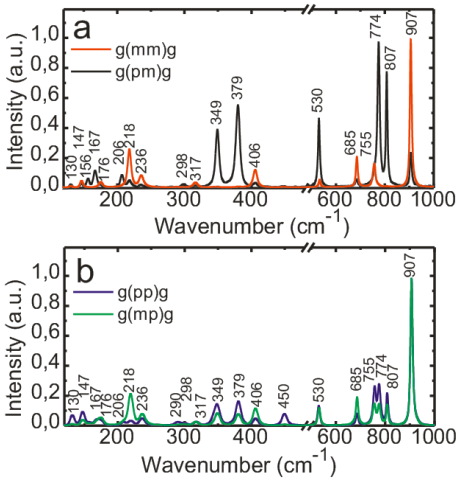

Fig. 7. Polarized Raman spectra of the Tm:KLuW crystal for the $g(xy)g$ geometries (where x and $y = m$ or p).

Table 1 Assignment of the Raman-active modes in Tm:KLuW

ν, cm^{-1}	Assignment*	ν, cm^{-1}	Assignment
907	ν(W–O) stretching	317	δ(WOW) bending
807		298, 290	
774	ν($W_0{}^0W$) stretching	236	T'(K^+) translational
755		218	T'(Lu^{3+}) translational
685		206	
530	ν(WOW) stretching	176	
450		167	T'(W^{6+}) translational
406		156	
379		147	
349	δ(OWO) bending	130	

*According to [46].

In Table 2, we have collected the main results regarding the CW Tm and Ho DT lasers reported so far in terms of their maximum output power P_{out} and slope efficiency η. A comparative plot of these parameters versus the laser wavelength λ_L is shown in Fig. 8. For KLuW crystals singly doped with Tm^{3+} ions, the tuning range of the laser emission is 1810–1982 nm (at zero-level, for $E \parallel N_m$). Power scaling of Tm:KLuW lasers up to few watts of output power was demonstrated with "bulk" laser elements, and even higher output powers reaching 5.9 W [26] and 10.4 W]28] were achieved with the thin-disk (TD) and mini-slab (MS) geometries, respectively.

Table 2 Selected results* on bulk CW Tm and Ho DT lasers reported so far

Crystal/scheme**	P_{out}, W	η, %	λ_L, nm	Ref.
Tm:KLuW / H	4.0	38	1950	[22]
Tm:KLuW / MS	10.4	43	1907	[28]
Tm:KLuW / TD	5.9	47	1855	[26]
Tm:KYW / M	2.2	74	1933–1944	[47]
Tm:KLuW / M	3.20	50.4	1946	[35]
Tm:KLuW / M+B	1.17	39	2109–2133	This work
Yb,Tm:KLuW / M	0.23	14	1983–2011	[21]
Ho:KLuW / H	0.51	67.6	2080	[48]
Ho:KLuW / M	0.53	88	2080	[49]
Tm,Ho:KLuW / M	0.45	31	2081	[9]

*P_{out} – maximum output power; η – slope efficiency with respect to absorbed pump power, λ_L – laser wavelength.
**H – hemispherical cavity, MS –microslab laser, TD – thin-disk, M – microchip; M+B – microchip with "bandpass" OC.

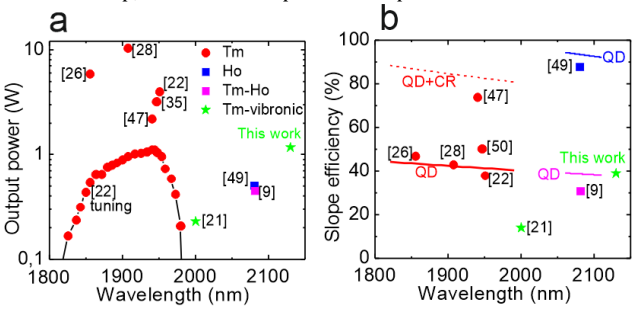

Fig. 8. Maximum CW output power (a) and laser slope efficiency η (b) versus the emission wavelength for Tm and Ho DT lasers reported so far; *solid curves*: – upper limit for η set by the quantum defect, λ_p/λ_L, (QD), *dashed curve*: upper limit set by the QD and CR.

Regarding the slope efficiency, it was normally higher than the limit set by the quantum defect, λ_p/λ_L ~40%, as shown by the solid lines in Fig. 8(b). This is due to a very efficient CR for adjacent Tm^{3+} ions, Fig. 6(a), whose quantum efficiency is very high in Tm:KLuW ($\eta_q > 1.9$) at reasonably low Tm^{3+} concentration of ~4×10^{20} at/cm^3 [6]. Thus, the generation of 2 photons at ~2 μm due to the absorption of one pump photon at ~0.8 μm is ideally expected from a highly-doped Tm:KLuW. The CR mechanism sets much higher limit for the laser slope efficiency, $2\lambda_p/\lambda_L$ ~80%, as indicated by the dashed curve in Fig. 8(b). For power-scaling experiments with the Tm:KLuW crystal, the longest emission wavelength was as short as ~1950 nm [22].

KLuW crystals singly doped with Ho^{3+} or codoped with Tm^{3+}/Ho^{3+} ions typically emit around 2080 nm, while their maximum slope efficiency varied from 88% to 31%, respectively. In the former case, the high slope efficiency was mainly due to the in-band pumping scheme [11,48] with a very low quantum defect. For Tm^{3+}, Ho^{3+} codoping, the laser efficiency is limited by the up-conversion losses [9]. The maximum output power of Ho DT lasers was limited to ~0.5 W.

Previous reports on Tm:DT vibronic lasers were devoted to the laser operation of Yb^{3+},Tm^{3+} codoped KLuW [18,21]. In [21], this laser generated 0.23 W at 1983–2011 nm with a very low slope efficiency of 14% mainly due to the strong up-conversion in this ion couple. The present results with the Tm:KLuW vibronic laser are superior compared to these earlier results. Moreover, the realized laser provides the longest emission wavelength ever achieved from any Tm or Ho DT laser, almost two times higher P_{out} compared to the Ho:DT lasers and similar η compared to the Tm DT lasers.

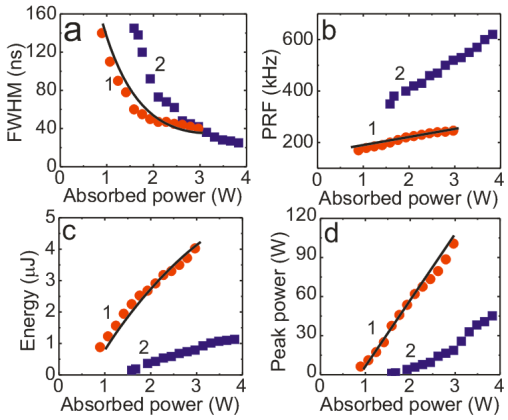

Fig. 9. SWCNT-SA PQS Tm:KLuW microchip laser: pulse duration (a), pulse repetition frequency, PRF, (b), pulse energy (c) and peak power (d) at 1.92 μm (10% OC) (1) and at 2.13 μm (1.6% "bandpass" OC) (2): *symbols* – experimental data, *curves* – numerical modeling.

The pulse characteristics of the PQS Tm:KLuW lasers are shown in Fig. 9. For both OCs used, the pulse duration τ decreased while both pulse repetition frequency (PRF) and pulse energy E_{out} increased with absorbed pump power. At 1.92 μm (10% OC), the duration got shorter from 140 to 40 ns while the PRF increased almost linearly in the 170–246 kHz range. The E_{out} varied in the range 0.9–4.0 μJ. Thus, the maximum peak power ($P_{peak} = E_{out}/\tau$) reached ~0.1 kW, a record value for bulk lanthanide lasers PQS by carbon nanostructures.

PQS was also achieved with the "bandpass" OC, at 2.13 μm. τ varied in the 145–25 ns range corresponding to a PRF of 350–620 kHz. An increased PRF resulted in lower pulse energies, E_{out} = 0.15–1.13 μJ and the peak power reached ~45 W at the maximum pump level.

The pulse characteristics of the PQS Tm:KLuW laser using 10% OC were simulated with the model of a quasi-three-level laser and a "fast" SA, see details in [50]. The absorption saturation of the SWCNT SA was described in accordance with Eq. (1). The parameters of the laser crystal and the SA involved in this modeling are listed in Table 3. The results are plotted in Fig. 9 as solid curves. The modeling agrees reasonably with the pulse characteristics dependence on the pump power. At P_{abs} = 2.9 W, the model predicts the generation of 35 ns / 4.6 μJ pulses corresponding to a PRF = 260 kHz which is in good agreement with the experimental data, cf. Fig. 9.

The oscilloscope traces of the shortest pulses generated by the PQS Tm:KLuW laser when using the two OCs are shown in Fig. 10(a). The pulses exhibit a nearly Gaussian temporal shape. The r.m.s. pulse-to-pulse timing jitter (the deviation of the pulse-to-pulse spacing from the average pulse period) was ~15% at 2.13 μm ("bandpass" OC) and even lower (<10%) at 1.92 μm (10% OC). A typical oscilloscope trace of the pulse train corresponding to the 10% OC is presented in Fig. 10(b). The pulse-to-pulse intensity instabilities in the pulse train were <15%. They are attributed to the heating of the SA by residual (non-absorbed) pump [39]. That could be avoided with suitable coatings on the crystal end-face enabling retro-reflection of the pump. It should be noted that this detrimental effect is less significant for the SWCNT SA as compared with graphene. For graphene SA, heating causes a distortion or buckling of the carbon layer due to the mismatch of thermal expansion coefficients for the layer/silica substrate [39]. For spaghetti-like SWCNTs, as in the present case, heating is less pronounced because the individual nanotubes are randomly oriented. No damage of the SWCNT-SA was observed in our experiments.

Table 3 Parameters of the Tm:KLuW laser crystal and the SWCNT saturable absorber

Parameter	Value
Tm:KLuW [23]	
Tm^{3+} concentration	$N_{Tm} = 2.15\times10^{20}$ cm^{-3}
Absorption cross-section (mean)	$\langle\sigma^{p}_{abs}\rangle = 1.60\times10^{-20}$ cm^2
SE cross-section ($E \parallel N_m$)	$\sigma^{L}_{SE} = 1.36\times10^{-20}$ cm^2
Reabsorption cross-section ($E \parallel N_m$)	$\sigma^{L}_{abs} = 0.17\times10^{-20}$ cm^2
Lifetime of Tm^{3+} ions	$\tau_l(^3F_4) = 0.80$ ms
Refractive index ($E \parallel N_m$)	$n_{AM} = 1.9918$
Thickness (along N_g-axis)	$t_{AM} = 3.0$ mm
Internal loss	$\delta = 0.0030$ cm^{-1}
SWCNT-SA [40,44]	
Saturation intensity	$I_{sat} = 7\pm1$ MW/cm^2
Small-signal absorption	$\alpha'_{SA} = 2.5\%$
Modulation depth	$\alpha'_{S} = 0.52\%$
Recovery time	$\tau_1 = 0.25$ ps; $\tau_2 = 1.16$ ps
Refractive index (SiO_2)	$n_{SA} = 1.4392$
Thickness (SiO_2)	$t_{SA} = 1.0$ mm

The output of the Tm:KLuW laser for both CW and PQS operation modes was nearly circular with $M^2_{xy} < 1.15$ ($x = m, y = p$), as measured in agreement with the ISO 11146-1 standard. This is attributed mainly to the low astigmatism of the thermal lens in this crystal [42].

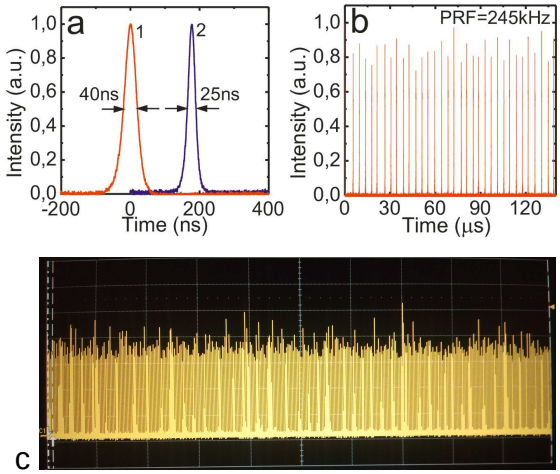

Fig. 10. SWCNT-SA PQS Tm:KLuW microchip laser: (a) Oscilloscope records of the shortest pulses achieved at 1.92 μm (10% OC) (1) and at 2.13 μm (1.6% "bandpass" OC) (2); (b) typical pulse train at 1.92 μm (10% OC) at P_{abs} = 2.9 W; (c) stability of the pulse train at 2.13 μm (1.6% "bandpass" OC) at P_{abs} = 3.8 W, total time window is 0.5 ms.

Table 4 Summary* of the Tm and Ho bulk lasers PQS with carbon nanostructures (graphene and SWCNTs) reported so far

Gain material	P_{out}, mW	τ, ns	E_{out}, μJ	P_{peak}, W	Ref.
SA: graphene					
Tm:CLNGG	40	9000	6.9	0.77	[52]
Tm:YAG	38	2080	1.74	0.84	[51]
Tm:LSO	106	7800	14	1.8	[53]
Tm:KLuW	34	3700	1	0.27	[54]
	310	285	1.6	5.6	[39]
Ho:YAG	572	632	**13.3**	21	[55]
Ho:YAG ceramic	264	2600	9.3	3.6	[56]
	640	170	3.6	21	[44]
Ho:LuAG	370	785	7.8	10	[57]
Tm,Ho:KLuW	74	200	0.2	1.0	[58]
SA: SWCNTs					
Tm:KLuW	**990**	40	4.0	**100**	This work
	700	**25**	1.1	45	This work
Tm,Ho:YAP	660	135	2.7	20	[59]
Ho:YAG ceramic	810	85	4.9	58	[44]

*P_{out} – maximum average output power; τ – pulse duration, E_{out} – pulse energy, P_{peak} – peak power. The best characteristics are selected if multiple results were reported. Bold numbers – record pulse characteristics.

In Table 4, we compared the pulse characteristics reported so far for bulk Tm and Ho lasers PQS by carbon nanostructures (graphene and SWCNTs). When using long cavities, such lasers generated pulses with duration τ ranging from few hundreds of ns to few μs, consequently the peak power P_{peak} was relative low (few watts). In the present work, we report on the shortest pulses (25 ns) ever achieved from bulk lanthanide lasers PQS by carbon nanostructures. As a result, P_{peak} increased one or two orders of magnitude, reaching the ~0.1 kW level. Moreover, the average output power generated by the Tm:KLuW laser PQS by SWCNTs approached ~1 W, higher than in any of the previous works. These improvements are attributed to several factors. First, the use of a microchip set-up enabled a significant shortening of the cavity roundtrip time. Second, the SWCNT SA possesses higher saturable absorption α'_S and smaller ratio α'_{NS}/α'_S than graphene, which is beneficial for the generation of shorter pulses. Third, laser operation in a long-wavelength region eliminates the impact of reabsorption losses in the crystal. Finally, as it is well-known for lasers PQS by carbon nanostructures ("fast" SAs) [44,50], the pulse characteristics depend significantly on how many times above threshold the laser is operating. In particular, the pulse duration shortens and the pulse energy increases. In our case, the realization of an efficient and power-scalable laser allowed us to utilize all these features.

Regarding the vibronic laser operation with Tm:KLuW crystals, further improvement in terms of extending the emission range due to electron-phonon coupling with the high energy phonons and an increase of the slope efficiency due to a more efficient CR both seem feasible with highly doped (10–25 at.%) Tm crystals. In this way, by further reduction of heat loading, power scaling of the vibronic Tm:KLuW lasers will be possible. As a consequence, these laser sources may compete with Ho DT lasers due to a simpler pump scheme and even broader wavelength tunability of the emission.

Concerning the utilization of SWCNTs as SA for ~2 μm lasers, they have high potential in comparison with semiconductor saturable absorber mirrors (SESAMs) due to the much easier and reproducible synthesis technology. Tm lasers PQS by SESAMs can generate pulses with pulse duration of few ns and energies of few μJ at PRFs in the MHz-range [47]. We believe that similar and even better characteristics are achievable with SWCNTs. Further shortening of the laser pulses may be reached either by shortening of the cavity length, e.g. by direct deposition of SWCNTs onto the crystal surface and reduction of the crystal length, which is feasible for highly-doped Tm:KLuW, or by an increase of the modulation depth of the SWCNT SA, e.g. by increasing their concentration.

4. CONCLUSION

In conclusion, we report on laser oscillation relying on vibronic interaction in Tm:KLuW, at wavelengths as long as ~2131 nm, extending those typical for Ho^{3+}-doped KLuW (2080 nm). This provides an extraordinary broad (290 nm, from 1.84 to 2.13 μm) range of laser emission in Tm:KLuW. The vibronic laser is passively Q-switched with a SWCNT SA to generate 25 ns / 1.1 μJ pulses at a repetition rate of 0.62 MHz. This represents the shortest duration ever achieved in bulk lasers Q-switched with carbon nanostructures (graphene or SWCNTs) and the longest wavelength at which SWCNT-SAs have been successfully applied so far. Operating the laser at 1919 nm, the pulse energy was scaled to 4 μJ and the maximum average output power reached ~1 W. These results could be improved by direct deposition of the SWCNT-SA on the crystal and by higher doping (>10 at.% Tm) of a thinner Tm:KLuW crystal to reduce the cavity length.

Funding. Spanish Government (MAT2013-47395-C4-4-R, TEC2014-55948-R); Generalitat de Catalunya (2014SGR1358).

Acknowledgment. F.D. acknowledges additional support through the ICREA academia award 2010ICREA-02 for excellence in research. X.M. acknowledges support from the European Union's Horizon 2020 research and innovation programme under the Marie Skłodowska-Curie grant agreement No 657630.

References

1. K. Scholle, S. Lamrini, P. Koopmann, and P. Fuhrberg, "2 μm laser sources and their possible applications," in *Frontiers in Guided Wave Optics and Optoelectronics*, B. Pal, ed., Intech, Vukovar, Croatia, (2010), pp. 471–500.
2. P. A. Budni, L. A. Pomeranz, M. L. Lemons, C. A. Miller, J. R. Mosto, and E. P. Chicklis, "Efficient mid-infrared laser using 1.9-μm-pumped Ho:YAG and $ZnGeP_2$ optical parametric oscillators," J. Opt. Soc. Am. B **17**, 723-728 (2000).
3. R. C. Stoneman, and L. Esterowitz, "Efficient, broadly tunable, laser-pumped Tm:YAG and Tm:YSGG cw lasers," Opt. Lett. **15**, 486–488 (1990).
4. T. Y. Fan, G. Huber, R. L. Byer, P. Mitzscherlich, "Continuous-wave operation at 2.1 μm of a diode-laser-pumped, Tm-sensitized Ho:$Y_3Al_5O_{12}$ laser at 300 K," Opt. Lett. **12**, 678-680 (1987).
5. P.A. Budni, M.L. Lemons, J.R. Mosto, and E.P. Chicklis, "High-power/high-brightness diode-pumped 1.9-μm thulium and resonantly pumped 2.1-μm holmium lasers," IEEE J. Select. Top. Quantum Electron. **6**, 629-635 (2000).
6. K. van Dalfsen, S. Aravazhi, C. Grivas, S. M. García-Blanco, and M. Pollnau, "Thulium channel waveguide laser with 1.6 W of output power and ~80% slope efficiency," Opt. Lett. **39**, 4380–4383 (2014).
7. S. A. Payne, L.L. Chase, L. K. Smith, W. L. Kway and W. F. Krupke, "Infrared cross- section measurement for crystals doped with Er^{3+}, Tm^{3+}, Ho^{3+}", IEEE J. Quantum Electron. **28**, 2619–2630 (1992).
8. T. Y. Fan, G. Huber, R. L. Byer, P. Mitzscherlich, "Spectroscopy and diode laser-pumped operation of Tm,Ho:YAG," IEEE J. Quantum Electron. **24**, 924–933 (1988).
9. P. Loiko, J.M. Serres, X. Mateos, K. Yumashev, N. Kuleshov, V. Petrov, U. Griebner, M. Aguiló, and F. Díaz, "Microchip laser operation of Tm,Ho: $KLu(WO_4)_2$ crystal," Opt. Express **22**, 27976-27984 (2014).
10. D.Y. Shen, A. Abdolvand, L.J. Cooper, W.A. Clarkson, "Efficient Ho:YAG laser pumped by a cladding-pumped tunable Tm:silica-fibre laser," Appl. Phys. B **79**, 559-561 (2004).

11. P. Loiko, J.M. Serres, X. Mateos, K. Yumashev, N. Kuleshov, V. Petrov, U. Griebner, M. Aguiló, and F. Díaz, "In-band-pumped Ho:KLu(WO_4)$_2$ microchip laser with 84% slope efficiency," Opt. Lett. **40**, 344–347 (2015).
12. F. Cornacchia, D. Parisi, C. Bernardini, A. Toncelli, and M. Tonelli, "Efficient, diode-pumped Tm^{3+}:BaY_2F_8 vibronic laser," Opt. Express **12**, 1982–1989 (2004).
13. F. Cornacchia, D. Parisi, and M. Tonelli, "Spectroscopy and diode-pumped laser experiments of $LiLuF_4$:Tm^{3+} crystals," IEEE J. Quantum Electron. **44**, 1076–1082 (2008).
14. N. Coluccelli, G. Galzerano, F. Cornacchia, A. Di Lieto, M. Tonelli, and P. Laporta, "High-efficiency diode-pumped Tm:$GdLiF_4$ laser at 1.9 µm," Opt. Lett. **34**, 3559–3561 (2009).
15. Y. F. Li, Y. Z.Wang, and B. Q. Yao, "Comparative optical study of thulium-doped $YAlO_3$ and $GdVO_4$ single crystals," Laser Phys. Lett. **5**, 37–40 (2008).
16. P. Koopmann, R. Peters, K. Petermann, and G. Huber, "Crystal growth, spectroscopy, and highly efficient laser operation of thulium-doped Lu_2O_3 around 2 µm," Appl. Phys. B **102**, 19–24 (2011).
17. C. Kränkel, "Rare-earth-doped sesquioxides for diode-pumped high-power lasers in the 1-, 2-, and 3-µm spectral range," IEEE J Sel. Top. Quantum Electron **21**, 1602013-1-13 (2015).
18. M. Segura, X. Mateos, M. C. Pujol, J. J. Carvajal, M. Aguiló, F. Díaz, U. Griebner, and V. Petrov, "Diode-pumped 2 µm vibronic (Tm^{3+}, Yb^{3+}): KLu(WO_4)$_2$ laser," Appl. Opt. **51**, 2701-2705 (2012).
19. A. Ellens, S. Schenker, A. Meijerink, and G. Blasse, "Vibronic transitions of Tm^{3+} in various lattices," J. Lumin. **69**, 1–15 (1996).
20. W.F. Krupke, "Optical absorption and fluorescence intensities in several rare-earth-doped Y_2O_3 and LaF_3 single crystals," Phys. Rev. **145**, 325-337 (1966).
21. P.A. Loiko, J.M. Serres, X. Mateos, M.P. Demesh, A.S. Yasukevich, K.V. Yumashev, V. Petrov, U. Griebner, M. Aguiló, and F. Díaz, "Spectroscopic and laser characterization of Yb,Tm:KLu(WO_4)$_2$ crystal," Opt. Mater. **51**, 223–231 (2016).
22. V. Petrov, M. C. Pujol, X. Mateos, Ò. Silvestre, S. Rivier, M. Aguiló, R. Solé, J. Liu, U. Griebner, and F. Díaz, "Growth and properties of KLu(WO_4)$_2$, and novel ytterbium and thulium lasers based on this monoclinic crystalline host," Laser Photonics Rev. 1, 179 (2007).
23. O. Silvestre, M.C. Pujol, M. Rico, F. Güell, M. Aguiló, and F. Díaz, "Thulium doped monoclinic KLu(WO_4)$_2$ single crystals: growth and spectroscopy," Appl. Phys. B **87**, 707–716 (2007).
24. A. E. Troshin, V. E. Kisel, A. S. Yasukevich, N. V. Kuleshov, A. A. Pavlyuk, E. B. Dunina, and A. A. Kornienko, "Spectroscopy and laser properties of Tm:KY(WO_4)$_2$ crystal," Appl. Phys. B. **86**, 287–292 (2007).
25. P.A. Loiko, S.M. Vatnik, I.A. Vedin, A.A. Pavlyuk, K.V. Yumashev, and N.V. Kuleshov, "Thermal lensing in N_m-cut monoclinic Tm:KLu(WO_4)$_2$ laser crystal," Laser Phys. Lett. **10**, 125005 -1-6 (2013).
26. S. Vatnik, I. Vedin, M. Segura, X. Mateos, M. C. Pujol, J. J. Carvajal, M. Aguiló, F. Díaz, V. Petrov, and U. Griebner, "Efficient thin-disk Tm-laser operation based on Tm:KLu(WO_4)$_2$/KLu(WO_4)$_2$ epitaxies," Opt. Lett. **37**, 356-358 (2012).
27. X. Mateos, V. Petrov, J. Liu, M.C. Pujol, U. Griebner, M. Aguilo, F. Diaz, M. Galan, and G. Viera, "Efficient 2-µm continuous-wave laser oscillation of Tm^{3+}:KLu(WO_4)$_2$," IEEE J. Quantum Electron. **42**, 1008–1015 (2006).
28. S. M. Vatnik, I. A. Vedin, and A. A. Pavlyuk, "High-efficiency 5%Tm: KLu(WO_4)$_2$ N_m-cut minislab laser," Laser Phys. Lett. **9**, 765–769 (2012).
29. M. Segura, M. Kadankov, X. Mateos, M. C. Pujol, J. J. Carvajal, M. Aguiló, F. Díaz, U. Griebner, and V. Petrov, "Passive Q-switching of the diode pumped Tm^{3+}: KLu(WO_4)$_2$ laser near 2-µm with Cr^{2+}:ZnS saturable absorbers," Opt. Express **20**, 3394-3400 (2012).
30. P. Loiko, J.M. Serres, X. Mateos, K. Yumashev, A. Yasukevich, V. Petrov, U. Griebner, M. Aguiló, and F. Díaz, "Sub-nanosecond Tm:KLuW microchip laser Q-switched by a Cr:ZnS saturable absorber," Opt. Lett. **40**, 5220-5223 (2015).
31. A. Schmidt, S. Y. Choi, D. Il Yeom, F. Rotermund, X. Mateos, M. Segura, F. Diaz, V. Petrov, and U. Griebner, "Femtosecond pulses near 2 µm from a Tm:KLuW laser mode-locked by a single-walled carbon nanotube saturable absorber," Appl. Phys. Express **5**, 092704-1–3 (2012).
32. Ò. Silvestre, J. Grau, M. C. Pujol, J. Massons, M. Aguiló, F. Díaz, M. T. Borowiec, A. Szewczyk, M. U. Gutowska, M. Massot, A. Salazar, and V. Petrov, "Thermal properties of monoclinic KLu(WO_4)$_2$ as a promising solid state laser host," Opt. Express **16**, 5022-5034 (2008).
33. P.A. Loiko, K.V. Yumashev, N.V. Kuleshov, G.E. Rachkovskaya, and A.A. Pavlyuk, "Detailed characterization of thermal expansion tensor in monoclinic KRE(WO_4)$_2$ (where Re = Gd, Y, Lu, Yb)," Opt. Mater. **34**, 23–26 (2011).
34. P.A. Loiko, K.V. Yumashev, N.V. Kuleshov, G.E. Rachkovskaya, and A.A. Pavlyuk, "Thermo-optic dispersion formulas for monoclinic double tungstates KRe(WO_4)$_2$ where Re = Gd, Y, Lu, Yb," Opt. Mater. **33**, 1688–1694 (2011).
35. J. M. Serres, X. Mateos, P. Loiko, K. Yumashev, N. Kuleshov, V. Petrov, U. Griebner, M. Aguiló, and F. Díaz, "Diode-pumped microchip Tm:KLu(WO_4)$_2$ laser with more than 3 W of output power," Opt. Lett. **39**, 4247-4250 (2014).
36. J. J. Zayhowski, "Microchip lasers," Opt. Mater. **11**, 255-267 (1999).
37. J. J. Zayhowski, and C. Dill, "Diode-pumped passively Q-switched picosecond microchip lasers," Opt. Lett. **19**, 1427-1429 (1994).
38. M. Gaponenko, N. Kuleshov, and T. Sudmeyer, "Efficient diode-pumped Tm:KYW 1.9-µm microchip laser with 1 W cw output power," Opt. Express **22**, 11578-11582 (2014).
39. J.M. Serres, P. Loiko, X. Mateos, K. Yumashev, U. Griebner, V. Petrov, M. Aguiló, and F. Díaz, "Tm:KLu(WO_4)$_2$ microchip laser Q-switched by a graphene-based saturable absorber," Opt. Express **23**, 14108-14113 (2015).
40. W. B. Cho, J. H. Yim, S. Y. Choi, S. Lee, A. Schmidt, G. Steinmeyer, U. Griebner, V. Petrov, D.-I. Yeom, K. Kim, and F. Rotermund, "Boosting the nonlinear optical response of carbon nanotube saturable absorbers for broadband mode-locking of bulk lasers," Adv. Funct. Mater. **20**, 1937-1943 (2010).
41. J. H. Yim, W. B. Cho, S. Lee, Y. H. Ahn, K. Kim, H. Lim, G. Steinmeyer, V. Petrov, U. Griebner, and F. Rotermund, "Fabrication and characterization of ultrafast carbon nanotube saturable absorbers for solid-state laser mode locking near 1 µm," Appl. Phys. Lett. **93**, 161106-1-3 (2008).
42. P. A. Loiko, J. M. Serres, X. Mateos, K. V. Yumashev, N. V. Kuleshov, V. Petrov, U. Griebner, M. Aguiló, and F. Díaz, "Characterization of thermal lens in Tm:KLu(WO_4)$_2$ and microchip laser operation," Laser Phys. Lett. **11**, 075001-1-7 (2014).
43. M. S. Dresselhaus, G. Drresselhaus, R. Saito, and A. Jorio, "Raman spectroscopy of carbon nanotubes," Physics Reports **409**, 47-99 (2005).
44. R. Lan, P. Loiko, X. Mateos, Y. Wang, J. Li, Y. Pan, S. Y. Choi, M. H. Kim, F. Rotermund, A. Yasukevich, K. Yumashev, U. Griebner, and V. Petrov, "Passive Q-switching of microchip lasers based on Ho:YAG ceramic," Appl. Opt., *to be published* (2016).
45. W. B. Cho, A. Schmidt, J. H. Yim, S. Y. Choi, S. Lee, F. Rotermund, U. Griebner, G. Steinmeyer, V. Petrov, X. Mateos, M. C. Pujol, J. J. Carvajal, M. Aguiló, and F. Díaz, "Passive mode-locking of a Tm-doped bulk laser near 2 µm using a carbon nanotube saturable absorber," Opt. Express **17**, 11007-11012 (2009).
46. L. Macalik, P.J. Deren, J. Hanuza, W. Strek, A.A. Demidovich, and A.N. Kuzmin, "Effect of random distribution and molecular interactions on optical properties of Er^{3+} dopant in KY(WO_4)$_2$ and Ho^{3+} in KYb(WO_4)$_2$," J. Mol. Struct. **450**, 179–192 (1998).
47. M. Gaponenko, N. Kuleshov, and T. Südmeyer, "Passively Q-switched thulium microchip laser," IEEE Photon. Technol. Lett. **28**, 147–150 (2016).
48. V. Jambunathan, X. Mateos, M. C. Pujol, J. J. Carvajal, M. Aguilo, F. Diaz, U. Griebner, and V. Petrov, "Optimization of dopant concentration in Ho:KLu(WO_4)$_2$ laser achieving ~70% slope efficiency," Laser Phys. **23**, 125801-1-4 (2013).
49. P. Loiko, J. M. Serres, X. Mateos, K. Yumashev, A. Malyarevich, A. Onushchenko, V. Petrov, U. Griebner, M. Aguiló, and F. Díaz,

"Ho:KLu(WO_4)$_2$ microchip laser Q-switched by a PbS quantum-dot-doped glass," IEEE Photon. Technol. Lett. **27**, 1795–1798 (2015).
50. P.A. Loiko, J.M. Serres, X. Mateos, J. Liu, H. Zhang, A.S. Yasukevich, K.V. Yumashev, V. Petrov, U. Griebner, M. Aguiló, and F. Díaz, "Passive Q-switching of Yb bulk lasers by a graphene saturable absorber," Appl. Phys. B **122**, 105-1-8 (2016).
51. Q. Wang, H. Teng, Y. W. Zou, Z. G. Zhang, D. H. Li, R. Wang, C. Q. Gao, J. J. Lin, L. W. Guo, and Z. Y. Wei, "Graphene on SiC as a Q-switcher for a 2 μm laser," Opt. Lett. **37**, 395–397 (2012).
52. G. Q. Xie, J. Ma, P. Lv, W. L. Gao, P. Yuan, L. J. Qian, H. H. Yu, H. J. Zhang, J. Y. Wang, and D. Y. Tang, "Graphene saturable absorber for Q-switching and mode locking at 2 μm wavelength," Opt. Mater. Express **2**, 878–883 (2012).
53. T. L. Feng, S. Z. Zhao, K. J. Yang, G. Q. Li, D. C. Li, J. Zhao, W. C. Quiao, J. Hou, Y. Yang, J. L. He, L. H. Zheng, Q. G. Wang, X. D. Xu, L. B. Su, and J. Xu, "Diode-pumped continuous wave tunable and graphene Q-switched Tm:LSO laser," Opt. Express **21**, 24665–24673 (2013).
54. J. M Serres, X. Mateos, U. Griebner, V. Petrov, M. Aguiló, and F. Díaz, "Single-layer graphene saturable absorber for diode-pumped passively Q-switched Tm:KLu(WO_4)$_2$ laser at 2 μm," Laser Phys. Lett. **12**, 095802-1-5 (2015).
55. C. J. Jin, X. M. Chen, L. F. Li, M. Qi, Y. Bai, Z. Y. Ren, and J. T. Bai, "A graphene-based passively Q-switched Ho:YAG laser in-band pumped by a diode-pumped Tm:YLF solid-state laser," Laser Phys. **24**, 035801-1–5 (2014).
56. T. Zhao, Y. Wang, H. Chen, and D. Shen, "Graphene passively Q-switched Ho:YAG ceramic laser," Appl. Phys. B **116**, 947–950 (2014).
57. Z. Cui, B. Yao, X. Duan, Y. Du, S. Xu, and Y. Wang, "Stable passively Q-switched Ho:LuAG laser with graphene as a saturable absorber," Opt. Eng. **53**, 126112-1–5 (2014).
58. J. M. Serres, P. Loiko, X. Mateos, V. Jambunathan, K. Yumashev, U. Griebner, V. Petrov, M. Aguiló, and F. Díaz, "Q-switching of a Tm,Ho: KLu(WO_4)$_2$ microchip laser by a graphene-based saturable absorber," Laser Phys. Lett., **13**, 025801-1 –5 (2016).
59. T. L. Feng, S. Z. Zhao, K. J. Yang, G. Q. Li, D. C. Li, J. Zhao, W. C. Qiao, L. H. Zheng, J. Xu, G. J. Zhao, and Y. G. Wang, "A diode-pumped passively Q-switched Tm,Ho:YAP laser with a single-walled carbon nanotube," Laser Phys. Lett. **10**, 095001-1–6 (2013).